Supporting Information for

Unveiling Heterogeneity of Interfacial Water through the Water Bending Mode

Takakazu Seki,[1,‡] Shumei Sun,[1,2,‡] Kai Zhong,[1] Chun-Chieh Yu,[1] Kevin Machel,[1] Lisa B. Dreier,[1] Ellen H. G. Backus,[1,2] Mischa Bonn,[1] and Yuki Nagata[1,*]

1. Max Planck Institute for Polymer Research, Ackermannweg 10, D-55128, Mainz, Germany

2. Department of Physical Chemistry, University of Vienna, Währinger Strasse 42, 1090 Vienna, Austria

[*]Correspondence: nagata@mpip-mainz.mpg.de

[‡]These authors are equally contributed.

SFG Measurements

SFG measurements were performed on a femtosecond Ti: Sapphire amplified laser system (Coherent Libra, ~800 nm, ~50 fs, 1 kHz) with 5 W output power. We used 2 W to pump an optical parametric amplifier (TOPAS, light conversion) with a noncolinear DFG stage to generate the broadband IR pulse. Another 1 W of the laser output was passed through an etalon to generate the narrowband visible pulse (~20 cm^{-1}). The visible and IR beams overlapped spatially and temporally at the sample surface with their incident angles of 64^0 and 40^0 with respect to the surface normal, respectively. Subsequently, the SFG signal is dispersed in a spectrometer and detected by an EMCCD camera. The visible and IR beams had pulse energies of roughly 10 μJ and 1 μJ, respectively, at the sample position. All the spectra are taken in the *ssp* (denoting *s*-, *s*-, and *p*-polarized SFG, visible and IR, respectively) polarization combination and normalized to the non-resonant signal taken from *z*-cut quartz after subtracting a background spectrum. We measured the SFG signal for 20 min at the water/DPTAP interface, 2×20 min at the water/DPPG, and 6×20 min at the water/air interfaces. For all the samples, we started the measurements after 7.5 min flushing with N_2.

Sample Preparation

We dissolved DPPG (sodium salt) and DPTAP (chloride salt) obtained from Avanti Polar Lipids in a mixture of 90% chloroform (Fischer Scientific, stabilized with amylene, >99%) and 10% methanol (VWR Chemicals, 99.8%) at a concentration of 4.3×10^{-4} mol/L. Sodium chloride (Sigma Aldrich, >99.5%) was baked in an oven for 8 hours at 650 °C. D_2O (>99.9%) was purchased from Eurisotop and used as received. H_2O is ultra-pure water from a MilliQ machine (18.2 MΩ cm). The solutions were poured into a rotating trough.[48] For generating the water/charged lipid interfaces, a controlled amount of lipid solution was added onto the solution using a click syringe. The surface area per lipid was 78 Å^2 for both DPTAP and DPPG.

Supplementary Method 1. Fitting Procedure for SFG Spectra of Water Bending Mode at Water/DPPG Interface

We performed the spectral fitting for the SFG spectra of H_2O/DPPG and D_2O/DPPG interfaces via;

$$\left|\chi^{(2)}_{\text{eff}}(\omega)\right|^2 = \left|A_{NR}e^{i\phi_{NR}} + \chi^{(2)}_{\text{C=O}}(\omega) + \chi^{(2)}_{\text{bend}}(\omega) + \chi^{(3)}_{\text{bend}}(\omega)\,\Phi(\sigma,c)\frac{\kappa(c)}{\kappa(c) - i\Delta k_z}\right|^2 \tag{S1}$$

and

$$\left|\chi^{(2)}_{\text{eff}}(\omega)\right|^2 = \left|A_{NR}e^{i\phi_{NR}} + \chi^{(2)}_{\text{C=O}}(\omega)\right|^2, \tag{S2}$$

respectively. Here, A_{NR} (ϕ_{NR}) and $\chi^{(2)}_{\text{C=O}}(\omega)$ are the amplitude (phase) of the non-resonant contribution and the second-order susceptibility of the C=O stretch mode of DPPG carbonyl group, respectively. $\chi^{(2)}_{\text{bend}}(\omega)$ and $\chi^{(3)}_{\text{bend}}(\omega)$ represent the second-order and third-order susceptibilities of the H-O-H bending mode, respectively. σ and c represent surface charge density and ion concentration, respectively. $\Phi(\sigma,c)$ is the surface potential, and $\kappa(c)$ is

inverse of the Debye length. Δk_z denotes the mismatch of the wave-vectors along z axis in the reflected SFG configuration.

In the Gouy-Chapman model, the surface potential $\Phi(\sigma,c)$ is given by[2]

$$\Phi_0(\sigma,c) = \frac{2k_BT}{e_c}\sinh^{-1}\left(\frac{\sigma}{\sqrt{8000k_BTN_A\varepsilon_0\varepsilon_r c}}\right) = 0.052 \cdot \sinh^{-1}\left(\frac{\sigma}{0.117\sqrt{c}}\right). \quad \text{(S3)}$$

The inverse of the Debye length $\kappa(c)$ is given by[2]

$$\kappa(c) = \sqrt{\frac{2000e_c^2N_Ac}{\varepsilon_0\varepsilon_r k_BT}} = \frac{\sqrt{c}}{0.304}, \quad \text{(S4)}$$

where k_B, T, e_c, N_A, ε_0, and ε_r represent the Boltzmann constant, temperature, the elementary charge, the Avogadro's number, the vacuum permittivity, and the relative permittivity of water, respectively. The surface charge density (-0.20 C/m^2) was obtained from the lipid concentration (4.3×10^{-4} mol/L, 25 μL) and the surface area of the trough (8 cm in a diameter). The mismatch of the wave-vectors, Δk_z, was calculated via;

$$\Delta k_z = k_{SFG,z} + k_{vis,z} + k_{IR,z}, \quad \text{(S5)}$$

and $k_{i,z} = \frac{2\pi}{\lambda}\sqrt{n_i^2 - sin^2\theta_i}$ $(i = SFG, vis, \text{or } IR)$, (S6)

where $k_{i,z}$, λ, n_i, and θ_i indicate wave-vector at z-plane for the beam (i), wavelength, refractive index of water corresponding to the beam (i), and beam angle with respect to the surface normal, respectively. We obtained $\Delta k_z = 1/56$ (nm^{-1}).

For each resonant vibrational contribution ($\chi^{(2)}_{C=O}(\omega)$, $\chi^{(2)}_{bend}(\omega)$, and $\chi^{(3)}_{bend}(\omega)$), we assumed the Lorentzian shapes of

$$\chi^{(2)}_{C=O}(\omega) = \frac{A_{C=O}}{\omega - \omega_{C=O} + i\Gamma_{C=O}},$$

(S7)

$$\chi^{(2)}_{\mathrm{bend}}(\omega) = \frac{A_{\mathrm{bend}(\chi^{(2)})}}{\omega - \omega_{\mathrm{bend}(\chi^{(2)})} + i\Gamma_{\mathrm{bend}}},$$

(S8) $$\chi^{(3)}_{\mathrm{bend}}(\omega) = \frac{A_{\mathrm{bend}(\chi^{(3)})}}{\omega - \omega_{\mathrm{bend}(\chi^{(3)})} + i\Gamma_{\mathrm{bend}}}.$$

(S9)

We conducted the global fitting for SFG spectra at H_2O/DPPG and D_2O/DPPG interfaces with various ion concentrations under some constraints. The phase of the non-resonant contribution (ϕ_{NR}) was set to be the same for fitting the spectra. For the C=O stretching mode contribution ($\chi^{(2)}_{\mathrm{C=O}}(\omega)$), $\omega_{\mathrm{C=O}}$ and $\Gamma_{\mathrm{C=O}}$ were shared between H_2O/DPPG and D_2O/DPPG interfaces. For the water bending mode contributions ($\chi^{(2)}_{\mathrm{bend}}$ and $\chi^{(3)}_{\mathrm{bend}}$), we use the same parameters for all the ion concentrations. Furthermore, we made a constraint that $\mathrm{Im}\left(\chi^{(2)}_{\mathrm{C=O}}\right)$ is positive.[3] This constraint allows us to determine the sign of the $A_{\mathrm{bend}(\chi^{(2)})}$ and $A_{\mathrm{bend}(\chi^{(3)})}$ uniquely. Finally, we obtained spectra of $\chi^{(2)}_{\mathrm{bend}}(\omega) = \frac{-6.8}{\omega - 1653 + 25i}$ and $\chi^{(3)}_{\mathrm{bend}}(\omega) = \frac{-44.2}{\omega - 1655 + 25i}$, where the unit of ω is cm^{-1}. The other obtained parameters are listed in Table S1.

In the previous SFG study on water/charged lipids interfaces,[3] Dreier and co-workers found two peaks for the C=O stretch mode of the lipid; one is a positive ~1720 cm^{-1} peak with large amplitude, while the other is a negative ~1740 cm^{-1} peak with small amplitude. Here, we used only a positive peak for the fit, because this is the dominant contribution for the C=O stretch mode. Furthermore, since we focus on the water bending mode at ~1650 cm^{-1}, the ~1740 cm^{-1} peak does not affect the fitting. As such, to reduce the degrees of freedom for the fitting, we used only one Lorentzian for the C=O stretch mode. Nevertheless, we note that there is a small discrepancy between our fit with one Lorentzian for the C=O stretch mode and the experimental data, which is marked by the arrows in Figure S1. This signifies the existence of the 1740 cm^{-1} peak for the C=O stretch mode.

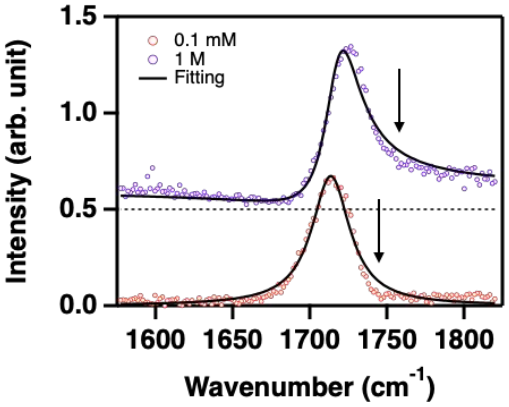

Figure S1. SFG spectra at the D_2O/DPPG interface at the concentrations of 0.1 mM and 1 M NaCl. These spectra are offset for clarity. The solid black lines indicate fits to the model using one Lorentzian mode for C=O stretch mode. Arrows in the plot indicate the discrepancy of the fits and the measured spectra.

Table S1. Fitting parameters for the vibrational SFG spectra at the water/DPPG interface with various ion concentrations.

D_2O	0.1 mM	1 mM	10 mM	0.1 M	0.25 M	1 M
A_{NR}	0.00 ± 0.01	0.02 ± 0.01	0.03 ± 0.01	-0.04 ± 0.01	-0.14 ± 0.01	-0.32 ± 0.01
ϕ_{NR} (rad)	-0.40	-0.40	-0.40	-0.40	-0.40	-0.40
$A_{C=O}$	-12.4 ± 0.3	-10.8 ± 0.3	-9.7 ± 0.3	-8.7 ± 0.3	-11.1 ± 0.3	-9.7 ± 0.2
$\omega_{C=O}$ (cm^{-1})	1713.6 ± 0.4	1713.4 ± 0.4	1713.8 ± 0.5	1714.3 ± 0.5	1718.3 ± 0.3	1717.5 ± 0.2
$\Gamma_{C=O}$ (cm^{-1})	15.1 ± 0.4	13.8 ± 0.4	13.9 ± 0.4	15.1 ± 0.6	14.9 ± 0.4	14.0 ± 0.3
H_2O						
A_{NR}	0.15 ± 0.01	0.11 ± 0.01	-0.01 ± 0.01	-0.15 ± 0.01	-0.27 ± 0.01	-0.42 ± 0.01
ϕ_{NR} (rad)	-0.40	-0.40	-0.40	-0.40	-0.40	-0.40
$A_{C=O}$	-11.6 ± 0.3	-9.6 ± 0.3	-10.2 ± 0.3	-9.39 ± 0.4	-10.9 ± 0.3	-9.4 ± 0.2
$\omega_{C=O}$ (cm^{-1})	1713.6 ± 0.4	1713.4 ± 0.4	1713.8 ± 0.5	1714.3 ± 0.5	1718.3 ± 0.3	1717.5 ± 0.2
$\Gamma_{C=O}$ (cm^{-1})	15.1 ± 0.4	13.8 ± 0.4	13.9 ± 0.4	15.1 ± 0.6	14.9 ± 0.4	14.0 ± 0.3

Supplementary Method 2. Fitting Procedure for SFG Spectra of Water Bending Mode at Water/DPTAP Interface

We further performed the fit of the SFG spectra at the water/DPTAP interface with various ion concentrations. For this fitting, we needed to introduce another vibrational resonance ($\chi^{(2)}_{1784\mathrm{cm}^{-1}}$) to adequately describe the broad peak at ~1784 cm^{-1}, in addition to the $\chi^{(2)}_{\mathrm{C=O}}(\omega)$, $\chi^{(2)}_{\mathrm{bend}}(\omega)$, and $\chi^{(3)}_{\mathrm{bend}}(\omega)$ contributions as well as the non-resonant contribution.[3] The spectra were fitted with the equations as below.

$$\left|\chi^{(2)}_{\mathrm{eff}}(\omega)\right|^2 = \left|A_{NR}e^{i\phi_{NR}} + \chi^{(2)}_{\mathrm{C=O}}(\omega) + \chi^{(2)}_{1784\mathrm{cm}^{-1}}(\omega) + \chi^{(2)}_{\mathrm{bend}}(\omega) + \chi^{(3)}_{\mathrm{bend}}(\omega)\Phi(\sigma)\frac{\kappa}{\kappa - i\Delta k_z}\right|^2, \tag{S10}$$

and

$$\left|\chi^{(2)}_{\mathrm{eff}}(\omega)\right|^2 = \left|A_{NR}e^{i\phi_{NR}} + \chi^{(2)}_{\mathrm{C=O}}(\omega) + \chi^{(2)}_{1784\mathrm{cm}^{-1}}(\omega)\right|^2. \tag{S11}$$

For the $\chi^{(2)}_{1784\mathrm{cm}^{-1}}(\omega)$ contribution, we assumed the Lorentzian shape of

$$\chi^{(2)}_{1784\mathrm{cm}^{-1}}(\omega) = \frac{A_{1784\mathrm{cm}^{-1}}}{\omega - 1784 + i\Gamma_{1784\mathrm{cm}^{-1}}}, \tag{S12}$$

where the $\chi^{(2)}_{\mathrm{C=O}}(\omega)$, $\chi^{(2)}_{\mathrm{bend}}(\omega)$, and $\chi^{(3)}_{\mathrm{bend}}(\omega)$ contribution employs the forms expressed by Eq. (S7)-(S9).

In analogous to the fit for the SFG spectra at the water/DPPG interface, we also used the constraints for the fit. We linked the phase information of the non-resonant contribution, ϕ_{NR} in each spectrum. For the C=O stretching mode contribution ($\chi^{(2)}_{\mathrm{C=O}}(\omega)$), $\omega_{\mathrm{C=O}}$ and $\Gamma_{\mathrm{C=O}}$ were shared between the H_2O/DPTAP and D_2O/DPTAP interfaces. For $\chi^{(2)}_{1784\mathrm{cm}^{-1}}(\omega)$ contribution, $\Gamma_{1784\mathrm{cm}^{-1}}$ was shared for the spectra with various ion concentrations. Furthermore, we used the same $A_{\mathrm{bend}(\chi^{(3)})}$ and $\omega_{\mathrm{bend}(\chi^{(3)})}$ values for the $\chi^{(3)}_{\mathrm{bend}}$ spectrum at the water/DPTAP interface as those at the water/DPPG interface. This is rationalized by taking into account the fact that the $\chi^{(3)}_{\mathrm{bend}}$ spectrum is governed by the bulk properties and not affected by the surface properties.[4] For the water bending mode contributions ($\chi^{(2)}_{\mathrm{bend}}$ and $\chi^{(3)}_{\mathrm{bend}}$

), we use the same parameters for all the ion concentrations. Under these constraints, our fit provided spectra of $\chi^{(2)}_{\text{bend}}(\omega) = \frac{1.5}{\omega - 1645 + 35i}$ and $\chi^{(3)}_{\text{bend}}(\omega) = \frac{-44.2}{\omega - 1655 + 35i}$ for the water/DPTAP interface. The other obtained parameters are listed in Table S2.

Table S2. Fitting parameters of the vibrational SFG spectra at the water/DPTAP interface with various ion concentrations.

D_2O	0.1 mM	1 mM	10 mM	0.1 M	1 M
A_{NR}	-0.78 ± 0.01	-0.75 ± 0.01	-0.57 ± 0.01	-0.46 ± 0.01	-0.43 ± 0.01
ϕ_{NR} (rad)	-0.68 ± 0.01	-0.68 ± 0.01	-0.68 ± 0.01	-0.68 ± 0.01	-0.68 ± 0.01
$A_{C=O}$	-6.9 ± 0.3	-8.5 ± 0.3	-7.7 ± 0.2	-7.7 ± 0.2	-11.0 ± 0.2
$\omega_{C=O}$ (cm^{-1})	1716.0 ± 0.3	1716.4 ± 0.3	1716.0 ± 0.3	1715.7 ± 0.3	1717.1 ± 0.2
$\Gamma_{C=O}$ (cm^{-1})	15.5 ± 0.5	14.8 ± 0.4	14.0 ± 0.3	13.1 ± 0.3	13.5 ± 0.3
$A_{1784\ cm^{-1}}$	-6.1 ± 0.8	-8.2 ± 1.0	-4.5 ± 0.7	-2.8 ± 0.7	-0.0 ± 0.7
$\Gamma_{1784\ cm^{-1}}$ (cm^{-1})	52.9 ± 4.8	52.9 ± 4.8	52.9 ± 4.8	52.9 ± 4.8	52.9 ± 4.8
H_2O					
A_{NR}	-0.53 ± 0.01	-0.56 ± 0.01	-0.50 ± 0.01	-0.45 ± 0.01	-0.41 ± 0.01
ϕ_{NR} (rad)	-0.68 ± 0.01	-0.68 ± 0.01	-0.68 ± 0.01	-0.68 ± 0.01	-0.68 ± 0.01
$A_{C=O}$	-6.8 ± 0.3	-8.1 ± 0.3	-8.5 ± 0.3	-9.6 ± 0.2	-9.6 ± 0.2
$\omega_{C=O}$ (cm^{-1})	1716.0 ± 0.3	1716.4 ± 0.3	1716.0 ± 0.3	1715.7 ± 0.3	1717.1 ± 0.2
$\Gamma_{C=O}$ (cm^{-1})	15.5 ± 0.5	14.8 ± 0.4	14.0 ± 0.3	13.1 ± 0.3	13.5 ± 0.3
$A_{1784\ cm^{-1}}$	-11.0 ± 1.3	-8.3 ± 1.1	-6.8 ± 1.0	-4.8 ± 0.8	-5.3 ± 0.9
$\Gamma_{1784\ cm^{-1}}$ (cm^{-1})	52.9 ± 4.8	52.9 ± 4.8	52.9 ± 4.8	52.9 ± 4.8	52.9 ± 4.8

Supplementary Method 3. Fitting for SFG Spectra Water Bending Mode at Water/Air Interface

On the basis of previous studies,[5–8] we assumed that the SFG spectrum at the water/air interface was composed of two different water contributions with a positive sign (a water molecule with two hydrogen-bond donors, named as DD-type species) and with a negative sign (a water molecule with one donor and the free O-H group, named as D-type species). The DD-(D-)type species are known to provide a high (low) frequency of the H-O-H bending mode.[7] We performed the spectral fit of the SFG spectrum at the water/air interface using the equation described as

$$\left|\chi^{(2)}_{\text{eff}}(\omega)\right|^2 = \left|A_{NR}e^{i\phi_{NR}} + \chi^{(2)}_{\text{bend1}}(\omega) + \chi^{(2)}_{\text{bend2}}(\omega)\right|^2. \quad \text{(S13)}$$

For the fitting, we assumed Lorentzian model to describe the vibrational modes as

$$\chi^{(2)}_{\text{bend1}}(\omega) = \frac{A_{\text{bend1}}}{\omega - \omega_{\text{bend1}} + i\Gamma_{\text{bend1}}}, \quad \text{(S14)}$$

and

$$\chi^{(2)}_{\text{bend2}}(\omega) = \frac{A_{\text{bend2}}}{\omega - \omega_{\text{bend2}} + i\Gamma_{\text{bend2}}}. \quad \text{(S15)}$$

Under the constrains of $\Gamma_{\text{bend1}} = \Gamma_{\text{bend2}} = 65\ \text{cm}^{-1}$, we obtained the best fit parameter of $\chi^{(2)}_{\text{bend1}}(\omega) = \frac{5.4}{\omega - 1612 + 65i}$ and $\chi^{(2)}_{\text{bend2}}(\omega) = \frac{-9.2}{\omega - 1661 + 65i}$, respectively. This peak separation $|\omega_{\text{bend1}} - \omega_{\text{bend2}}|$ of ~50 cm^{-1} is well consistent with the previous simulation studies.[6–8] Although the obtained Γ_{bend1} and Γ_{bend2} are slightly larger than the reported fitting parameters (45-60 cm^{-1}),[5] the obtained ω_{bend2} shows good agreement with the previous experiment and simulation works.[5,6]

Supplementary Method 4. Relation of Bending Mode Frequency and Stretch Mode Frequency

The bending mode frequency (ω_b) and the stretch mode frequency (ω_s) averaged over the two O-H stretch vibrational frequency was given;[9]

$$\omega_b^{\mathrm{ref}} - \omega_b = -0.2583\left(\omega_s^{\mathrm{ref}} - \omega_s\right), \tag{S16}$$

where ω_b^{ref} and ω_s^{ref} are the reference frequencies of the bending and stretch modes, respectively. The coefficient of -0.2583 was also confirmed by the theory calculation,[6] whereas the choice of ω_b^{ref} and ω_s^{ref} is somehow arbitrary. For ω_b and ω_s close to the gas-phase water vibrational frequencies, ω_b^{ref} and ω_s^{ref} can be reasonably chosen from the gas-phase water vibration data (ω_b^{g} and ω_s^{g}) as;

$$\omega_b^{\mathrm{g}} - \omega_b = -0.2583\left(\omega_s^{\mathrm{g}} - \omega_s\right), \tag{S17}$$

On the other hand, for ω_b and ω_s close to the liquid-phase water vibrational frequencies, one should take the liquid water data of ω_b^{l} and ω_s^{l}.

$$\omega_b^{\mathrm{l}} - \omega_b = -0.2583\left(\omega_s^{\mathrm{l}} - \omega_s\right), \tag{S18}$$

Here, ω_b^{g}=1595 cm^{-1}, ω_s^{g} = 3710 cm^{-1}, ω_b^{l}=1650 cm^{-1},[10] ω_s^{l} = 3400 cm^{-1}.[11] Since equations (S17) and (S18) are not identical, we connected these two equations with a smoothing function in the frequency region of $\omega_b^{\mathrm{g}} < \omega_b \leq \omega_b^{\mathrm{l}}$, while (S18) was used for $\omega_b > \omega_b^{\mathrm{l}}$. The resulting functions for estimating the stretch mode frequency thus read;

$$\sin^2\varphi\left(\omega_b^{\mathrm{l}} - \omega_b\right) + \cos^2\varphi\left(\omega_b^{\mathrm{g}} - \omega_b\right) = -0.2583\left(\sin^2\varphi'\left(\omega_s^{\mathrm{l}} - \omega_s\right) + \cos^2\varphi'\left(\omega_s^{\mathrm{g}} - \omega_s\right)\right) \text{ for } \omega_b^{\mathrm{g}} < \omega_b \leq \omega_b^{\mathrm{l}},$$

$$\omega_b^{\mathrm{l}} - \omega_b = -0.2583\left(\omega_s^{\mathrm{l}} - \omega_s\right) \text{ for } \omega_b > \omega_b^{\mathrm{l}}, \tag{S19}$$

where $\varphi = \frac{\pi\omega_b - \omega_b^{\mathrm{g}}}{2\omega_b^{\mathrm{l}} - \omega_b^{\mathrm{g}}}$ and $\varphi' = \frac{\pi\omega_s - \omega_s^{\mathrm{g}}}{2\omega_s^{\mathrm{l}} - \omega_s^{\mathrm{g}}}$.

Supplementary Discussion 1. Density Functional Theory Calculation for Understanding the Relation of Water Orientation and Sign of Water Bend Mode SFG Signal

The relation of the water orientation and the sign of the SFG peak of the water bending mode, $\mathrm{Im}\left(\chi^{(2)}_{\mathrm{bend}}\right)$, is complicated, because of the induced effects of the dipole moment and polarizability. This has already been pointed out in the bulk; the different sign of the transition dipole moment for the permanent dipole moment and induced dipole moment, causing a smaller IR bending mode peak in ice than that in the liquid water.[12] The interplay of the transition dipole-moment and the polarizability is more complicated. Thus, to check the sign of the $\mathrm{Im}\left(\chi^{(2)}_{\mathrm{bend}}\right)$ at the water-DPPG and water-DPTAP conformations, we performed the density functional theory (DFT) calculations of water in various environments.

The DFT calculation was done with Gaussian 16.[13] First, we optimized the structure of a single water molecule, a water molecule hydrogen-bonded to two other water molecules, and a water molecule near the core parts of the DPPG and DPTAP headgroups (CH_3-O-PO_2-O-CH_3^- and N-$(CH_3)_4^+$). The level of the calculation was B3LYP/cc-pVTZ. The obtained coordinates are listed in Table S3-6, while their structures are displayed in Table S7. Subsequently, we computed the normal modes of water bending mode for geometry-optimized water molecules for these conformations. By using the normal modes, we computed the transition dipole moment and the transition polarizability at the B3LYP/aug-cc-pVTZ level of theory. The augmented function for the basis sets is crucial for computing the molecular polarizability.

The calculated transition dipole moment and polarizability of the water bending mode are summarized in Table S7. This table indicates that, when the orientation of the target water molecule is the same, the phase of the transition dipole moment is the same. However, the transition polarizability is not so simple; when a water molecule is a DD-type species (two hydrogen atoms are both hydrogen-bond donors), the magnitude of the negative $\frac{\partial \alpha_{\perp}}{\partial Q_{\mathrm{bend}}}$ is larger than that of the positive $\frac{\partial \alpha_{\parallel}}{\partial Q_{\mathrm{bend}}}$, while in other cases, the magnitude of the negative $\frac{\partial \alpha_{\perp}}{\partial Q_{\mathrm{bend}}}$ is smaller than that of the positive $\frac{\partial \alpha_{\parallel}}{\partial Q_{\mathrm{bend}}}$.

To connect these transition dipole moment and transition polarizability in the molecular frame with the SFG responses in the lab frame, one needs to take an ensemble average of the different water conformations by rotating the transition dipole moment and transition polarizability in the molecular frame. By assuming that the orientation of a water molecule is uniformly distributed in the lower half part of the sphere (see Figure S2), the SFG amplitude can be written as;

$$A^{(2)}_{\text{bend}} \propto \frac{1}{2}\left\langle \frac{\partial \mu_Z}{\partial Q_{\text{bend}}}\left(\frac{\partial \alpha_{XX}}{\partial Q_{\text{bend}}} + \frac{\partial \alpha_{YY}}{\partial Q_{\text{bend}}}\right)\right\rangle$$
$$= \frac{1}{2}\int_0^{\pi/2} \sin\theta \frac{\partial \mu_z}{\partial Q_{\text{bend}}} \cos\theta \left(\frac{\partial \alpha_{\perp}}{\partial Q_{\text{bend}}}\cos^2\theta + \frac{\partial \alpha_{\parallel}}{\partial Q_{\text{bend}}}\sin^2\theta\right) d\theta \propto \frac{\partial \mu_z}{\partial Q_{\text{bend}}}\left(\frac{\partial \alpha_{\perp}}{\partial Q_{\text{bend}}} + \frac{\partial \alpha_{\parallel}}{\partial Q_{\text{bend}}}\right),$$

(S20)

where $\alpha_{\parallel} = \alpha_{zz}$ and $\alpha_{\perp} = (\alpha_{xx} + \alpha_{yy})/2$, and ($X$, Y, Z) represents the lab-frame and (x, y, z) represents the molecular frame. Here, we used the relation of

$$\mu_{\text{lab}} = A\mu_{\text{mol}}$$

(S21)

$$\alpha_{\text{lab}} = A\alpha_{\text{mol}}A^{\dagger}$$

(S22)

where A is the rotation matrix converting from the molecular frame to the lab-frame.

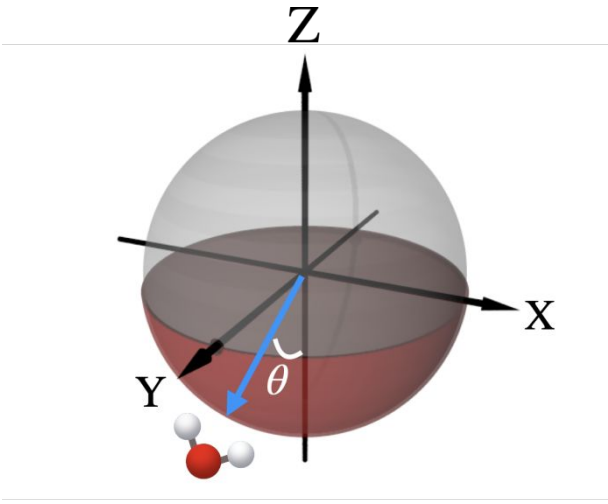

Figure S2. Low half sphere marked in red represents the area for the integration in Eq. (S20). The blue arrow shows direction of the transition dipole moment of water molecule. θ indicates the angle between the transition dipole moment and the Z-axis.

The sign of the SFG amplitude can be readily understood from the signs of $\frac{\partial \mu_Z}{\partial Q_{\text{bend}}}$ and $\frac{\partial \alpha_{\perp}}{\partial Q_{\text{bend}}} + \frac{\partial \alpha_{\parallel}}{\partial Q_{\text{bend}}}$ based on Eq. (S20). For a water molecule bonded to the two water molecules

(DD-type water molecule), *up*-(*down*-)orientation of the dipole moment of water provides the negative (positive) sign of the SFG amplitude. This is consistent with the SFG signal at the water-air interface.[6–8] On the other hand, the water molecule near the DPPG and DPTAP headgroups as well as the single gas-phase water molecule shows the opposite trend; the *up*-(*down*-) orientation of the dipole moment of water provides the positive (negative) sign of the SFG amplitude. Now, these data are compared with the sign of $\mathrm{Im}(\chi^{(2)}_{\mathrm{bend}})$ obtained from the experiments. Since the DPTAP is on the top of the water molecules at the water/DPTAP interface, the sign of the transition dipole moment of water should be flipped. Thus, Im $(\chi^{(2)}_{\mathrm{bend}})$ at the water/DPTAP interface should have a negative sign, based on Table S7. This is consistent with the negative $\mathrm{Im}(\chi^{(2)}_{\mathrm{bend}})$ obtained from the experiment. For the water/DPPG interface, Table S7 predicts the positive sign for $\mathrm{Im}(\chi^{(2)}_{\mathrm{bend}})$, again consistent with the experiment.

Table S3. Atom coordinates of `single gas-phase water molecule.`

Atom	X	Y	Z
O	0.0000	0.0000	0.0000
H	0.7534	0.1395	0.5924
H	-0.7534	0.0000	0.6086

Table S4. Atom coordinates of `a water molecule hydrogen-bonded to two water molecules.`

Atom	X	Y	Z
O	0.0000	0.0000	0.0000
H	0.7708	-0.0138	0.5809
H	-0.7708	0.0000	0.5813
O	-2.5908	0.8680	1.1186
H	-2.3624	1.5126	0.4467
H	-3.4582	0.5505	0.8667
O	2.6986	0.7155	0.9168
H	3.5820	0.3454	0.8871
H	2.6047	1.1767	0.0947

Table S5. Atom coordinates of a water molecule near the core part of the DPPG headgroup.

Atom	X	Y	Z
O	0.0000	0.0000	0.0000
H	-0.7358	0.0009	0.6350
H	0.7358	0.0000	0.6364
P	0.0154	0.7778	3.1152
O	1.2928	0.2527	2.5621
C	-1.0919	0.9354	5.4725
H	-0.9570	0.5555	6.4847
H	-1.2193	2.0194	5.5129
H	-1.9843	0.4922	5.0312
C	-0.4228	3.0523	1.8986
H	-1.5132	3.0754	1.8555
H	-0.0402	4.0729	1.9058
H	-0.0561	2.5410	1.0087
O	-1.2991	0.3130	2.5684
O	0.0598	0.5931	4.7314
O	0.0172	2.4219	3.0847

Table S6. Atom coordinates of a water molecule near the core part of the DPTAP headgroup.

Atom	X	Y	Z
O	0.0000	0.0000	0.0000
H	0.7611	0.0001	0.5909
H	-0.7611	0.0000	0.5907
C	0.2786	-0.0007	-5.1391
H	-0.1792	0.8894	-5.5613
H	-0.1802	-0.8905	-5.5611
H	1.3456	-0.0013	-5.3429
N	0.0671	-0.0004	-3.6526
C	0.6954	1.2279	-3.0497
H	1.7596	1.2171	-3.2691
H	0.2359	2.1071	-3.4930
H	0.5259	1.2063	-1.9768
C	-1.4055	0.0005	-3.3513
H	-1.8527	0.8907	-3.7848
H	-1.8537	-0.8893	-3.7845
H	-1.5338	0.0007	-2.2736
C	0.6940	-1.2292	-3.0494
H	0.2335	-2.1080	-3.4923
H	1.7582	-1.2197	-3.2688
H	0.5247	-1.2071	-1.9764

Table S7. Transition dipole moment, transition polarizability, and their product. The H-O-H angular bisector forms the *z*-axis.

	$\frac{\partial \mu_z}{\partial Q}$	$\frac{\partial \alpha_{\parallel}}{\partial Q}$	$\frac{\partial \alpha_{\perp}}{\partial Q}$	$\frac{\partial \mu_z}{\partial Q}\frac{\partial(\alpha_{\parallel}+\alpha_{\perp})}{\partial Q}$
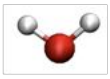	0.05	0.18	-0.06	0.006
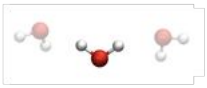	0.04	0.07	-0.16	-0.004
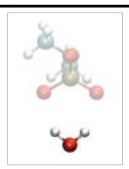	0.11	0.31	-0.27	0.004
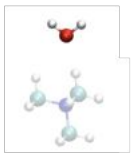	0.06	0.14	-0.06	0.005

Supplementary Discussion 2. Constructive vs Destructive Interference of Water Bending Mode and C=O Stretch Mode

From the fit of the SFG spectra, we have obtained the different sign of the bending mode contributions $(\chi^{(2)}_{\text{bend}}(\omega) + \chi^{(3)}_{\text{bend}}(\omega)\Phi(\sigma,c)\frac{\kappa(c)}{\kappa(c)-i\Delta k_z})$ at low ion concentrations. This can be confirmed not only from the fit but also from the lineshapes of the SFG intensity spectra through the interference of the bending mode contribution and the C=O stretch mode contribution. Here, by using the model calculations, we examine how the constructive interference (both bending mode and C=O stretch mode contributions have positive signs) and destructive interference (bending mode and C=O stretch mode contributions has negative and positive signs, respectively) affect the lineshape of the SFG spectra.

Figure S3 displays the imaginary part and real part spectra of two Lorentzians with resonant frequencies of 1655 and 1714 cm^{-1}. The linewidths were set to be 35 and 20 cm^{-1}, respectively. When destructive interference occurs between the bending mode and C=O stretch mode, the real part signal is enhanced in the frequency region between bending mode frequency and the C=O stretch frequency (see solid blue line in Figure S3(b)). In contrast,

when constructive interference occurs, real part signal is suppressed (see solid blue line in Figure S3(e)). As such, the resulting SFG intensity spectra show a shoulder for the bending mode region for the destructive interference (Figure S3(c)) and an independent peak for the constructive interference (Figure S3(f)).

Here, we turn our focus on the SFG spectra. Figure S4 shows the SFG spectra at the H_2O/DPPG and H_2O/DPTAP interfaces at 0.1 mM concentration. One can clearly see that the SFG spectrum at the H_2O/DPPG interface shows a shoulder, while the SFG spectrum at the H_2O/DPTAP interface exhibits an independent peak. Given that the sign of the C=O stretch mode peak in the $\mathrm{Im}\chi^{(2)}$ spectrum is positive,[3] the sign of the bending modes at the DPPG and DPTAP interfaces can be assigned to the negative and positive, respectively. Since the $\chi^{(3)}_{\mathrm{bend}}\Phi$ contribution is dominant at 0.1 mM concentration, one can conclude that the sign of $\mathrm{Im}\left(\chi^{(3)}_{\mathrm{bend}}\Phi\right)$ is negative at the DPPG interface and positive at the DPTAP interface. This is consistent with the fit results (see Figure 2(c) in the main text).

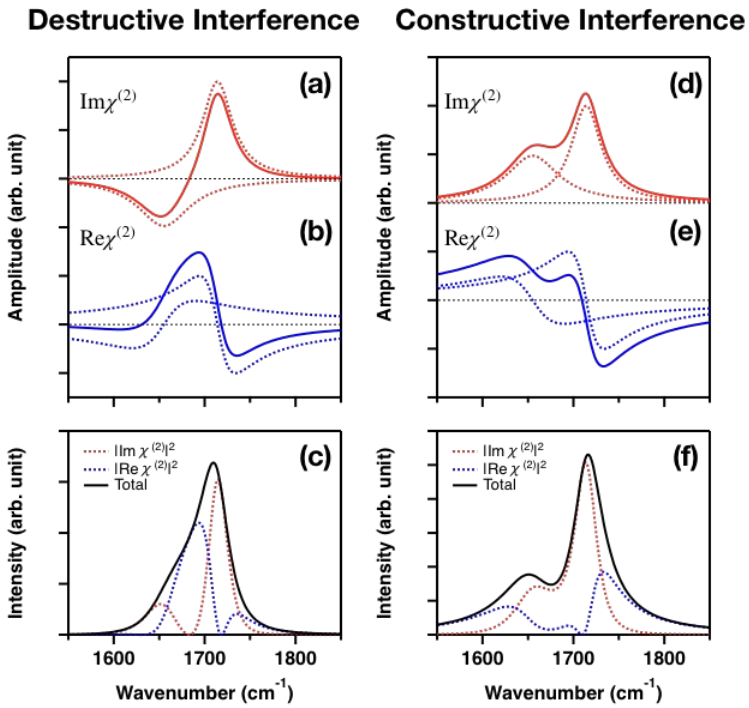

Figure S3. Destructive and constructive interference between two resonant vibrational modes. (a, b, d, e) The imaginary and real parts of simulated $\chi^{(2)}$spectra of two overlapping peaks with the opposite sign (destructive interference) (a, b) and the same sign (constructive interference) (d, e). (c, f) Intensity spectra $|\chi^{(2)}|^2$.

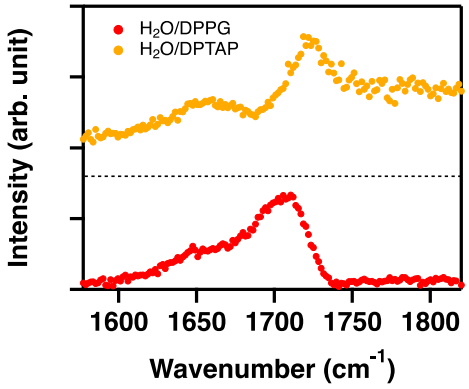

Figure S4. SFG spectra at the H_2O/DPPG and H_2O/DPTAP interfaces with a concentration of 0.1 mM NaCl solution. The spectra are offset for clarity.

Supplementary Discussion 3. Peak Shifts of C=O Stretching Mode

The other important consequence from the analysis in the Supplementary Discussion 1 is that the peak around 1710 cm^{-1} in the SFG intensity spectra is red-shifted from the frequency of the intrinsic C=O stretch mode for the destructive interference and is slightly blue-shifted for the constructive interference as shown in Figure S3(c, f). Since the intrinsic C=O stretch mode frequency can be obtained from the SFG spectra at the D_2O/DPPG and D_2O/DPTAP interfaces, comparison of the C=O stretch mode frequency between the SFG spectra of D_2O and H_2O provides the information on the destructive and constructive interference, clarifying the sign of the spectrum for the bending mode of water.

Figure S5 plots the frequency shift $\Delta\omega = \omega_{C=O,H_2O} - \omega_{C=O,D_2O}$ of the peaks for the C=O stretch mode at the water/DPPG and water/DPTAP interfaces. The water/DPPG interface clearly shows the negative $\Delta\omega$ at the ion concentration < 1 mM, while $\Delta\omega$ is positive at the ion concentration > 0.1 M. This strongly suggests that the sign of the water bending mode at the water/DPPG interface is changed by varying the ion concentration. This is consistent with the fit results. Because, a contribution from the peak at ~1784 cm^{-1} also affects the peak position of the C=O stretch mode for the water/DPTAP interface, it is not straightforward to connect $\Delta\omega$ with the sign of the bending mode peak.

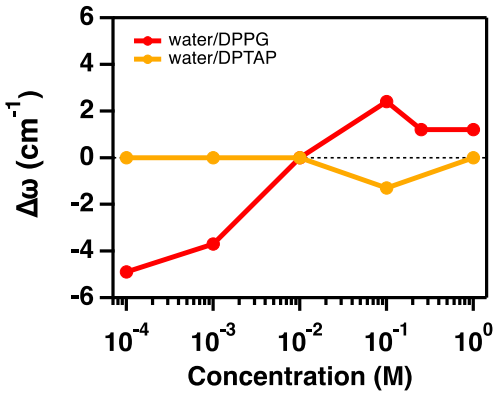

Figure S5. The frequency shift ($\Delta\omega$) of C=O stretch mode at the water/charged lipids interfaces vs. NaCl concentration.

Supplementary References

(1) Backus, E. H. G.; Bonn, D.; Cantin, S.; Roke, S.; Bonn, M. Laser-Heating-Induced Displacement of Surfactants on the Water Surface. *J. Phys. Chem. B* **2012**, *116*, 2703–2712.

(2) Bard, A. J.; Faulkner, L. R. *Electrochemical Methods: Fundamentals and Applications*; wiley New York, 2001; Vol. 2.

(3) Dreier, L. B.; Bonn, M.; Backus, E. H. G. Hydration and Orientation of Carbonyl Groups in Oppositely Charged Lipid Monolayers on Water. *J. Phys. Chem. B* **2019**, *123*, 1085–1089.

(4) Wen, Y.-C.; Zha, S.; Liu, X.; Yang, S.; Guo, P.; Shi, G.; Fang, H.; Shen, Y. R.; Tian, C. Unveiling Microscopic Structures of Charged Water Interfaces by Surface-Specific Vibrational Spectroscopy. *Phys. Rev. Lett.* **2016**, *116*, 016101.

(5) Dutta, C.; Benderskii, A. V. On the Assignment of the Vibrational Spectrum of the Water Bend at the Air/Water Interface. *J. Phys. Chem. Lett.* **2017**, *8*, 801–804.

(6) Ni, Y.; Skinner, J. L. IR and SFG Vibrational Spectroscopy of the Water Bend in the Bulk Liquid and at the Liquid-Vapor Interface, Respectively. *J. Chem. Phys.* **2015**, *143*, 014502.

(7) Nagata, Y.; Hsieh, C.-S.; Hasegawa, T.; Voll, J.; Backus, E. H. G.; Bonn, M. Water Bending Mode at the Water–Vapor Interface Probed by Sum-Frequency Generation Spectroscopy: A Combined Molecular Dynamics Simulation and Experimental Study. *J. Phys. Chem. Lett.* **2013**, *4*, 1872–1877.

(8) Moberg, D. R.; Straight, S. C.; Paesani, F. Temperature Dependence of the Air/Water Interface Revealed by Polarization Sensitive Sum-Frequency Generation Spectroscopy. *J. Phys. Chem. B* **2018**, *122*, 4356–4365.

(9) Falk, M. The Frequency of the H-O-H Bending Fundamental in Solids and Liquids. *Spectrochim. Acta* **1984**, *40*, 43–48.

(10) Maréchal, Y. IR Spectroscopy of an Exceptional H-Bonded Liquid: Water. *J. Mol. Struct.* **1994**, *322*, 105–111.

(11) Perakis, F.; Marco, L. De; Shalit, A.; Tang, F.; Kann, Z. R.; Kühne, T. D.; Torre, R.; Bonn, M.; Nagata, Y. Vibrational Spectroscopy and Dynamics of Water. *Chem. Rev.* **2016**, *116*, 7590–7607.

(12) Imoto, S.; Xantheas, S. S.; Saito, S. Molecular Origin of the Difference in the HOH Bend of the IR Spectra between Liquid Water and Ice. *J. Chem. Phys.* **2013**, *138*, 054506.

(13) Frisch, M. J.; Trucks, G. W.; Schlegel, H. B.; Scuseria, G. E.; Robb, M. A.; Cheeseman, J. R.; Scalmani, G.; Barone, V.; Petersson, G. A.; Nakatsuji, H.; Li, X.; Caricato, M.; Marenich, A. V.; Bloino, J.; Janesko, B. G.; et al. Gaussian 16. *Revis. A, Gaussian, Inc.* **2016**.